Experimental and Toxicologic Pathology 67 (2015) 323–329

Contents lists available at ScienceDirect

Experimental and Toxicologic Pathology

journal homepage: www.elsevier.de/etp

Enriched inorganic compounds in diesel exhaust particles induce mitogen-activated protein kinase activation, cytoskeleton instability, and cytotoxicity in human bronchial epithelial cells

Robson Seriani[a], Mara S. Junqueira[b], Claudia E. Carvalho-Sousa[c], Alessandra C.T. Arruda[d], Diana Martinez[e], Adriano M. Alencar[e], Ana L. Garippo[f], Jôse Mara Brito[a], Milton A. Martins[d], Paulo H.N. Saldiva[a], Elnara M. Negri[a], Thais Mauad[a], Mariangela Macchione[a,*]

[a] Laboratory of Experimental Air Pollution (LIM05), Department of Pathology, School of Medicine, University of São Paulo, São Paulo, Brazil
[b] Central Biotery Laboratory, School of Medicine, University of São Paulo, São Paulo, Brazil
[c] Laboratory of Chronopharmacology, Department of Physiology, Institute of Bioscience, University of São Paulo, São Paulo, São Paulo, Brazil
[d] Experimental Therapeutics Laboratory, Department of Medicine, School of Medicine, University of São Paulo, Brazil
[e] Laboratory of Microrheology and Molecular Physiology, Institute of Physics, University of São Paulo, São Paulo, Brazil
[f] PREMIUM Confocal Microscopy Core Facility, University of São Paulo, Brazil

ARTICLE INFO

Article history:
Received 9 January 2015
Accepted 20 February 2015

Keywords:
Diesel exhaust particles
Metals
MAPKs
Cytotoxicity
Cell viscoelasticity

ABSTRACT

This study assessed the effects of the diesel exhaust particles on ERK and JNK MAPKs activation, cell rheology (viscoelasticity), and cytotoxicity in bronchial epithelial airway cells (BEAS-2B). Crude DEP and DEP after extraction with hexane (DEP/HEX) were utilized. The partial reduction of some DEP/HEX organics increased the biodisponibility of many metallic elements. JNK and ERK were activated simultaneously by crude DEP with no alterations in viscoelasticity of the cells. Mitochondrial activity, however, revealed a decrease through the MTT assay. DEP/HEX treatment increased viscoelasticity and cytotoxicity (membrane damage), and also activated JNK. Our data suggest that the greater bioavailability of metals could be involved in JNK activation and, consequently, in the reduction of fiber coherence and increase in the viscoelasticity and cytotoxicity of BEAS cells. The adverse findings detected after exposure to crude DEP and to DEP/HEX reflect the toxic potential of diesel compounds. Considering the fact that the cells of the respiratory epithelium are the first line of defense between the body and the environment, our data contribute to a better understanding of the pathways leading to respiratory cell injury and provide evidence for the onset of or worsening of respiratory diseases caused by inorganic compounds present in DEP.

1. Introduction

Particulate matter or traffic-related particles are the major source of air pollution in urban environments, and have been associated with increased rates of hospital admissions, exacerbations of chronic obstructive pulmonary disease (COPD) and asthma, and low birth weight, as well as with cardiovascular, endocrine and reproductive disturbances and increased reports of cancer due to both organic and inorganic compounds (Saldiva et al., 2002; Pope and Dockery, 2006; Sérgio-Chiarelli et al., 2011; Altuğ et al., 2013; Gurbani et al., 2013; Gan et al., 2013; Miraglia et al., 2013; Romão et al., 2013; Yorifuji and Kashima, 2013; Schikowski et al., 2014; Cakmak et al., 2014).

The chemical composition and the particles found in DEPs vary according to engine type, operating conditions, fuel formulation

Abbreviations: DEP, diesel exhaust particles; DEP/HEX, diesel exhaust particles treated with hexane; MAPK, mitogen activated protein kinases; PAHs, polycyclic aromatic hydrocarbons; LDH, lactate dehydrogenase; ERK, extracellular regulated kinase; pERK, phosphorylated extracellular regulated kinase; JNK, c-Jun N-terminal kinase; pJNK, phosphorylated c-Jun N-terminal kinase; MTT, 3-(4,5-dimethylthiazol-2-yl)-2,5-diphenyltetrazolium bromide; $^*(f)$, complex apparent stiffness; Pa/nm, Pascal per nanometer; η, hysteresivity; G^*, the complex shear modulus; g', the elastic modulus; g'', the loss modulus; $|G^*|$, the complex modulus of G^*; G, $|G^*|$ at 0.75 Hz.

* Corresponding author at: Faculdade de Medicina USP, Departamento de Patologia, Av. Dr. Arnaldo 455, 1° andar, sala 1150, Cerqueira César, São Paulo, SP, CEP: 01246-903, Brazil. Tel.: +55 11 30618520.
E-mail address: mmacchione@lim05.fm.usp.br (M. Macchione).

http://dx.doi.org/10.1016/j.etp.2015.02.004
0940-2993/

(high-/low-sulfur fuel), and the duration of vehicle operation (Wichmann, 2007). Moreover, DEPs from vehicles are a major contributor to metals in air pollution, and their levels could be higher than those in gasoline exhausts (Lim et al., 2009). Several studies have hypothesized that low levels of these metals help to define the toxicity of particles. Their inflammatory effects can impair airway mucociliary clearance and acidification of intra-epithelial mucus, and can also lead to changes to the thickness of the pseudo-stratified ciliated epithelium (Laks et al., 2008; Yoshizaki et al., 2010; Seriani et al., 2014, 2015).

In vitro studies have shown that human bronchial epithelial cell exposure to DEP also decreases ciliary beat frequency and induces cytoskeleton stiffness, the activation of mitogen-activated protein kinase (MAPK), cytotoxic effects, and the release of inflammatory cytokines, all of which occur through apoptosis and reduction in cell viability (Bayram et al., 1998; Li et al., 2002; Abou Chakra et al., 2007; Papaharalambus and Griendling, 2007; Li et al., 2009; Totlandsdal et al., 2010; Wu et al., 2012; Totlandsdal et al., 2013; Seriani et al., 2014).

Abnormal regulation of the MAPK pathways has been reported in a wide range of diseases, including cancer, asthma, and COPD. MAPK extracellular regulated kinase (ERK)1/2 and c-Jun N-terminal kinase (JNK) have also been associated with changes to the cytoskeleton, and increases growth and metabolism to ERK and cell death to JNK (Barros and Marshall, 2005; Tricker et al., 2011; Wortzel and Seger, 2011).

DEP particles represent a complex mixture of organic and inorganic elements, but the contribution of inorganic components (particularly metals) to the cell injuries associated with DEP exposure is not clear. The metals found in particulate matter contribute to cardio-respiratory morbidity, and transition metals (such as iron) are known to participate in reactions that generate oxidative stress, leading to hospital admission in children as a result of respiratory distress, and cardiovascular mortality (Araujo and Nel, 2009; Ayres et al., 2008; Ghio et al., 2012; Li et al., 2003; Ostro et al., 2009; Zhou et al., 2010; Hsu et al., 2011).

Previous information indicates that MAPK could be activated by metals and could therefore lead to cytotoxicity. However, little is known about metals in the cellular structure or the role played by MAPK activation in these events has been reported.

In this study, we aimed to address the effects of DEP and to better understand how DEP treated with hexane (DEP/HEX) (to remove organic compounds), affects on cell rheology (viscoelasticity), cytotoxicity, and MAPK activation.

2. Methods

2.1. Diesel exhaust particulate (DEP) collection and characterization

Particles were collected after 1 day of routine operation of a bus running on Diesel S500 from the city of São Paulo's metropolitan fleet. The vehicle was equipped with a Mercedes Benz MB1620 210-hp engine with a Euro III emission profile, without electronic control of fuel injection or any post-treatment of emissions in the exhaust pipe. The collected diesel was stored for toxicological analysis as previously described (Laks et al., 2008). For the analysis of the metals Ni, S, Fe, V, Pb, Cd, Cr, and Cu, RX fluorescence spectrometry was used (EDX 700 HS, Shimatzu Corporation Analytical Instruments Division, Kyoto, Japan). PAH levels were evaluated by means of high-performance liquid chromatography. The concentrations of the following PAHs were determined: benzo[b]fluoranthene, benzo[k]fluoranthene, benzo[a]pyrene, dibenz[ab]anthracene, and indeno[123-cd]anthracene.

Table 1
Inorganic characterization of crude DEP and DEP treated with hexane (DEP/HEX).

Metals (ppm)	DEP	DEP/HEX
Nickel (Ni)	0.181 ± 0.037	0.319 ± 0.014
Sulfur (S)	0.626 ± 0.416	0.985 ± 0.145
Iron (Fe)	74.566 ± 2.266	63.996 ± 0.544
Vanadium (V)	0.037 ± 0.013	0.016 ± 0.021
Lead (Pb)	0.050 ± 0.047	0.037 ± 0.021
Cadmium (Cd)	0.029 ± 0.008	0.125 ± 0.044
Chrome (Cr)	0.161 ± 0.116	0.166 ± 0.023
Copper (Cu)	0.017 ± 0.001	0.147 ± 0.008

Table 2
Organic characterization (PHAs) in crude DEP and DEP treated hexane (DEP/HEX).

PHAs (ng/g)	DEP	DEP/HEX
Naphthalene	49.23	ND
Acenafetileno	179.48	5.08
Fluorene	683.94	45.75
Anthracene	94.73	ND
Pyrene	12,838.73	631.31
Benzo[a]anthracene	1162.73	107.23
Benzo[a]fluoranthene	789.93	201.21
Benzo[k]fluoranthene	562.28	10.58
Benzo[a]pyrene	1642.28	26.42

2.2. Particle treatment

Total mass of collected particles (8 g) was divided into two samples. One sample received no further treatment (DEP), and the other was extracted with following a protocol that removes organic compounds: Particles were immersed in 160 ml hexane (DEP/HEX), sonicated for 60 min, and left at rest for 24 h. Solutions were centrifuged for 15 min at 1811 × *g* at 10 °C. The supernatant was discarded, and the precipitate was stored in a vacuum dissector for 15 h. The metal content (ppm) and organic compounds (ng/g) of both intact diesel particles and content levels after the extraction procedures were described by Laks et al. (2008) (Tables 1 and 2). The fraction and the crude DEP were stored in a freezer at −20 °C until the experiments were performed.

2.3. Cell culture

The transwell was pre-coated with 10 μg/ml of Matrigel (BD Biosciences, Bedford, Massachusetts, USA) in the apical compartment. After 1 h at 37 °C, the Matrigel was washed and the BEAS-2B cells (kindly provided by Dr. M. Si-Tahar) were seeded onto the apical compartment (4×10^4) in 200 μl of modified LHC-9 growth medium with additives (Biosource) (0.5 ng/ml recombinant epidermal growth factor (EGF), 500 ng/ml hydrocortisone, 0.005 mg/ml insulin, 0.035 mg/ml bovine pituitary extract, 500 nM ethanolamine, 500 nM phosphoethanolamine, 0.01 mg/ml transferrin, 6.5 ng/ml 3,3′,5-triiodothyronine, 500 ng/ml epinephrine, 0.1 ng/ml retinoic acid, and trace elements). The growth medium was supplemented with: 10% inactivated FBS, 100 μl glutamine at 2 mM, 100 μl sodium pyruvate at 1 mM, 100 μl non-essential amino acids at 0.1 mM, 100 μl antibiotics at 0.1%. The basolateral compartment received 1000 μl of medium as well. After 72 h, when the cells reached 80% confluence, the medium was removed from the apical compartment and an air–liquid interface (ALI) was established. After 24 h in ALI, the cells were exposed to DEP and DEP/HEX.

2.4. Cell treatment

The cells were treated with: (a) 100 μg/ml of crude DEP; (b) 100 μg/ml of DEP treated with hexane (DEP/HEX); and (c) only

medium (control) after 15 and 30 min. Experiments were performed in triplicate.

2.5. Cytoskeleton integrity and cell size via immunofluorescence staining

After treatment, the cells that adhered to the transwell membrane were washed with the medium, placed in buffered 4% formaldehyde/PBS for 15 min for fixation, and then removed and placed in PBS for 24 h. Cells were then permeabilized in 0.2% Triton X-100/PBS and stained with 4′,6-diamidino-2-phenylindole (DAPI) for DNA visualization and with Phalloidin-Alexa-labeled (488 nm) for visualization of the cytoskeleton.

The transwell membranes were cut, fixed, and analyzed under a Zeiss 510 Meta confocal laser scanning microscope attached to a Zeiss Axiovert 200 M inverted microscope. Images were taken by using a 63× magnification immersion oil lens at a resolution of 512 × 512. Six fields with six cells were randomly chosen (Tamura et al., 2010) and were acquired to evaluate the expression of phalloidin.

Image analysis was performed using Image-J software. Phalloidin signal was used to evaluate the coherence of the actin fibers. We used the ImageJ Plugin, Orientation J, which evaluates the local orientation and two isotropic properties: the energy and the coherence coefficient of the image. A coherence coefficient closer to one indicates a strongly coherent orientation of the F-actin, whereas a coherence coefficient closer to zero denotes no preferential orientation of the fibers (Rezakhaniha et al., 2012).

2.6. Optical magnetic twisting cytometry (OMTC)

OMTC is a widely used method for the evaluation of the viscoelastic properties of individual adherent cells, such as human airway cells, vascular smooth muscle (HASM), or bronchial epithelial airway (BEA) cells (Fabry et al., 2001; Bursac et al., 2005; Berntsen et al., 2010; Park et al., 2010; Dinardo et al., 2013). In this method, a sinusoidal vertical magnetic field, here at 0.75 Hz, imposed a torque on previously horizontally magnetized ferromagnetic beads. The displacement of the beads was optically registered by a charge-coupled device camera mounted on an inverted microscope. Since the beads are intrinsically attached to cytoskeleton through Arg-Gly-Asp (RGD) coverage, the dynamics of the beads, resulting from the magnetic torque, are directly coupled with the viscoelastic properties of the cytoskeleton.

The ratio between torque and bead displacement defined the complex apparent stiffness of the cell, $g^*(f)$, which was measured in Pa/nm. With this value, it was possible to compute the elastic modulus g', the loss modulus g'', and the hysteresivity η (the ratio g''/g') of the cell. Apparent stiffness, or $g^*(f)$, was converted into a shear modulus G^* after considering the shape and thickness of the cell and the degree of bead embedding, $|G^*|$ at 0.75 Hz was labeled as G (Fabry et al., 2001; Bursac et al., 2005; Berntsen et al., 2010; Park et al., 2010; Zhou et al., 2012; Dinardo et al., 2013).

2.7. Cytotoxicity

Cytotoxicity was evaluated by quantifying the release of cytosolic enzyme lactate dehydrogenase (LDH) into the culture medium. The MTT assay is a colorimetric assay that measures the reduction of MTT via mitochondrial succinate dehydrogenase. LDH release assays are used to evaluate cell membrane integrity, and the colorimetric MTT assay measures mitochondrial reduction capacity. The cells were seeded into 96-well plates at a density of 5×10^4 cells/well and incubated for 24 h before treatment.

2.8. MTT assay

Briefly, the cells were seeded in 96-well plates containing 5×10^4 cells/well in 180-μl medium. The cells were cultured for 12 h to allow for attachment to the substrate. DEP was added at volumes of 5–250 μg/ml at 60 min to establish test concentration. The cells were then incubated with MTT (0.5 mg/ml) for 4 h at 37 °C, which was followed by dimethylsulfoxide (DMSO) exposure for 30 min under constant agitation. DMSO allows for solubilization of the formazan, a black compound that was quantified using a microplate spectrophotometer (Spectramax 250, Molecular Devices, California, USA) at 540 nm. Cell viability was defined as the percentage of optical density of each group compared to the control group.

2.9. LDH assay

The LDH assay is based on the reduction of nicotinamide adenine dinucleotide (NAD) to NADH by the lactate dehydrogenate. The resulting NADH is used in the stoichiometric conversion of a colored tetrazolium dye. The increase in LDH–NADH conversion is proportional to cell lysis (Riss and Moravec, 2004). The supernatant (30 μl) was filtered to remove DEP (0.22 μM, Millipore, MA, USA), transferred to a 96-well plate, and incubated with 170 μl of the substrate assay (200 mM NaCl, 19 mM $NaH_2PO_4 \cdot H_2O$, 81 mM $Na_2HPO_4 \cdot 7H_2O$, 0.2 mM NADH, and 1.6 mM pyruvate). A standard NADH curve was established, with duplicates of the eight points. The reaction was quantified at a wavelength of 340 nm in a microplate spectrophotometer (SpectraMAX250, Molecular Devices, California, USA) at different times (0, 5, 10 and 15 min, 37 °C) after incubation with the substrate.

2.10. Western blotting for ERK and JNK

After treatment, proteins were extracted with lysis buffer (Triton X-100 1%, NaCl 150 mM, Tris 50 mM pH 7.5, 1 mM Na_3VO_4, 1 mM PMSF, and 2 μg/ml aprotinin) (Sigma Chemical, St. Louis, MO). Protein concentration was determined using the BCA protein assay (Pierce, Rockford, IL). Equal amounts of protein (40 μg/ml) were separated by electrophoresis using 10% SDS-PAGE and were then transferred to PVDF membranes (Millipore). Blots were blocked with 5% BSA in TBST (Tris 25 mM, pH 7.8, NaCl 125 mM, and Tween-20 0.1%) (Sigma Chemical, St. Louis, MO) for 1 h. Next, the membranes were incubated overnight with anti-phospho-JNK1/2 antibodies (Calbiochem, San Diego, CA) and anti-phospho ERK1/2 (Calbiochem, San Diego, CA). The membranes were washed with TBST and were incubated with horseradish peroxidase-conjugated goat anti-rabbit IgG (Sigma Chemical, St. Louis, MO). The proteins were then visualized using ImageQuant LAS 4000 (GE, Fairfield, CT) through ECL detection reagents (GE Healthcare, Fairfield, CT). The same blot used for phosphorylated ERK was also used for total ERK. The same blot was used for β-actin and phosphorylated JNK. To ensure equal protein loading, the same blot was then incubated with anti-MAP kinase ERK1/2 (Calbiochem, San Diego, CA) and β-actin (Sigma Chemical, St. Louis, MO) and developed using a horseradish peroxidase-conjugated goat anti-rabbit IgG and horseradish peroxidase-conjugated anti-mouse IgG, respectively. After development, the bands were quantified via densitometry analysis.

2.11. Statistical analysis

Data distribution was tested for all variables using Kolmogorov–Smirnov analysis. Normally distributed variables were reported as mean ± standard error (SE), and significance was determined using the univariate general linear model (GLM)

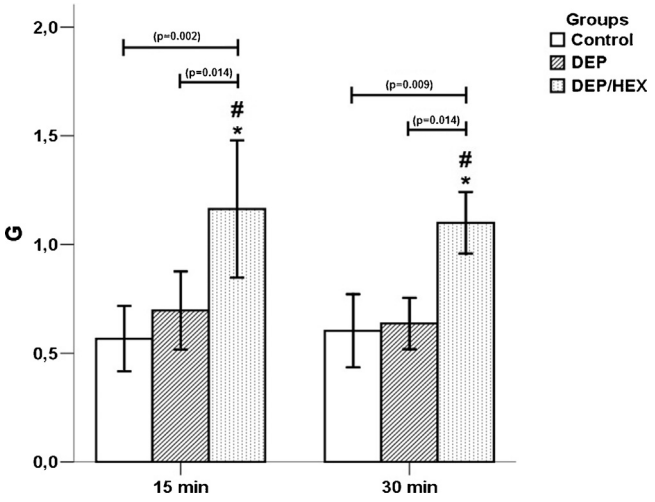

Fig. 1. Graphic representation of BEAS-2B rheology (viscoelasticity) (G) after treatment with crude DEP and DEP/HEX at 15 and 30 min. Cell viscoelasticity increased compared to the control after 15 min of exposure to DEP/HEX ($p = 0.002$) and crude DEP ($p = 0.014$). The treatment with DEP/HEX at 30 min was found to differ from the control ($p = 0.009$) and from crude DEP ($p = 0.014$).

for variance analysis of one dependent variable by two factors. The level of significance was set to 5%. Statistical analyses were performed using SPSS 15.0 (IBM).

3. Results

The treatment of diesel particles with hexane (DEP/HEX) decreased PAHs in 94%. The partial reduction in the concentrations of some PAHs and metals provided greater availability of some elements (see Table 1).

The cellular rheology was evaluated by measuring viscoelasticity (G). DEP/HEX increased the viscoelasticity significantly compared to the control ($p = 0.002$) and crude DEP after 15 min and 30 min ($p = 0.014$, $p = 0.014$, respectively). Fig. 1 shows BEAS-2B viscoelasticity (G) after crude DEP and DEP/HEX treatment after 15 and 30 min.

MTT assay and LDH assay are colorimetric assays for accessing cell viability and plasma membrane integrity, respectively. Crude DEP significantly reduced ($p = 0.001$) the MTT reaction at both times tested (15 and 30 min). No changes were observed after DEP/HEX stimulation (Fig. 2).

Lactate dehydrogenase (LDH) is rapidly released into the cell culture medium upon damage of the plasma membrane. DEP/HEX exposure caused a significant increase in lactate dehydrogenase release in the medium compared to the control and crude DEP after 15 and 30 min ($p = 0.001$) (Fig. 3).

The coherence coefficient quantification was verified as a parameter of cytoskeletal integrity. DEP/HEX treatment significantly ($p = 0.001$) affected fiber orientation in that it reduced the coherency coefficient of the actin fibers (15 and 30 min) (Fig. 4).

Immunoblotting data suggested that pERK and pJNK was activated by DEP treatments. Over time, crude DEP was found to induce the phosphorylation of ERK (pERK) (15 and 30 min) and of JNK (15 min); meanwhile, DEP/HEX did not cause ERK phosphorylation but it did cause JNK phosphorylation (pJNK) after 30 min of incubation (Fig. 5).

4. Discussion

In this study, we demonstrated that DEP and DEP/HEX differentially induce cytotoxicity, MAPK activation, and cytoskeleton disruption or alteration in fiber coherence in BEAS-2B cells. Both

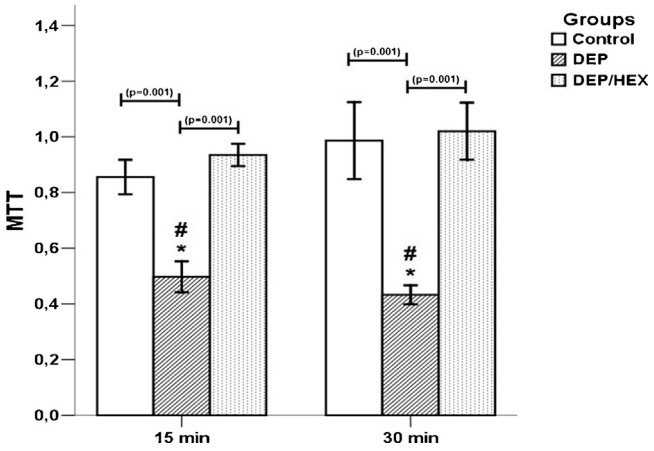

Fig. 2. Graphic representation of BEAS-2B shows cell viability via MTT assays (3-(4,5-dimethythiazol-2-yl)-2,5-diphenyl tetrazolium bromide) after treatment with crude DEP and DEP/HEX exposure at 15 and 30 min. Crude DEP differed from all treatments at 15 min ($p = 0.001$). Crude DEP at 30 min differed from the control and from DEP/HEX ($p = 0.001$).

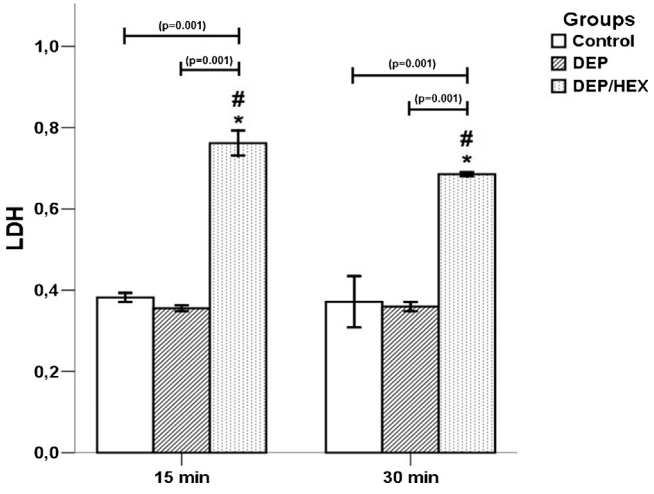

Fig. 3. Graphic representation of BEAS-2B shows cytotoxicity lactate dehydrogenase (LDH) after crude DEP and DEP/HEX exposure at 15 and 30 min. DEP/HEX exposure caused a significant increase in lactate dehydrogenase (LDH) release in the medium when compared to the control and to crude DEP at 15 and 30 min ($p = 0.001$).

crude DEP and DEP/HEX-treated cells had negative effects on cell viability (MTT or LDH), but only DEP/HEX altered cytoskeleton integrity and viscoelasticity.

Diesel particle extraction caused differences in particle toxicity indicators in BEAS-2B cells. The organic compounds decreased as a result of DEP/HEX extraction procedures (Table 2). The concentration of some elements (S, Ni, Cd, Cr and Cu) in DEP/HEX increased because of the relative enrichment of the inorganic fraction due to the removal of part of the organic fraction (Laks et al., 2008). Studies have shown that transition metals, such as Cu, and Ni, present in DEPs can produce reactive oxygen species (ROS) or can catalyze the formation of H_2O_2. These compounds trigger a cellular response mediated by the activation of intracellular signaling pathways, which culminate in proliferation, cell transformation, or cell death (Fantl et al., 1993; Dreher et al., 1996; Hill and Treisman, 1995; Ghio et al., 2002).

BEAS-2B cells exposed to crude DEP did not present differences in fiber coherence. There was a decrease in MTT assay over time, with no increases in LDH. Our data suggest that exposure to DEP decreases mitochondrial activity without significant alterations to the cytoskeleton or to cell rheology. It is possible that the

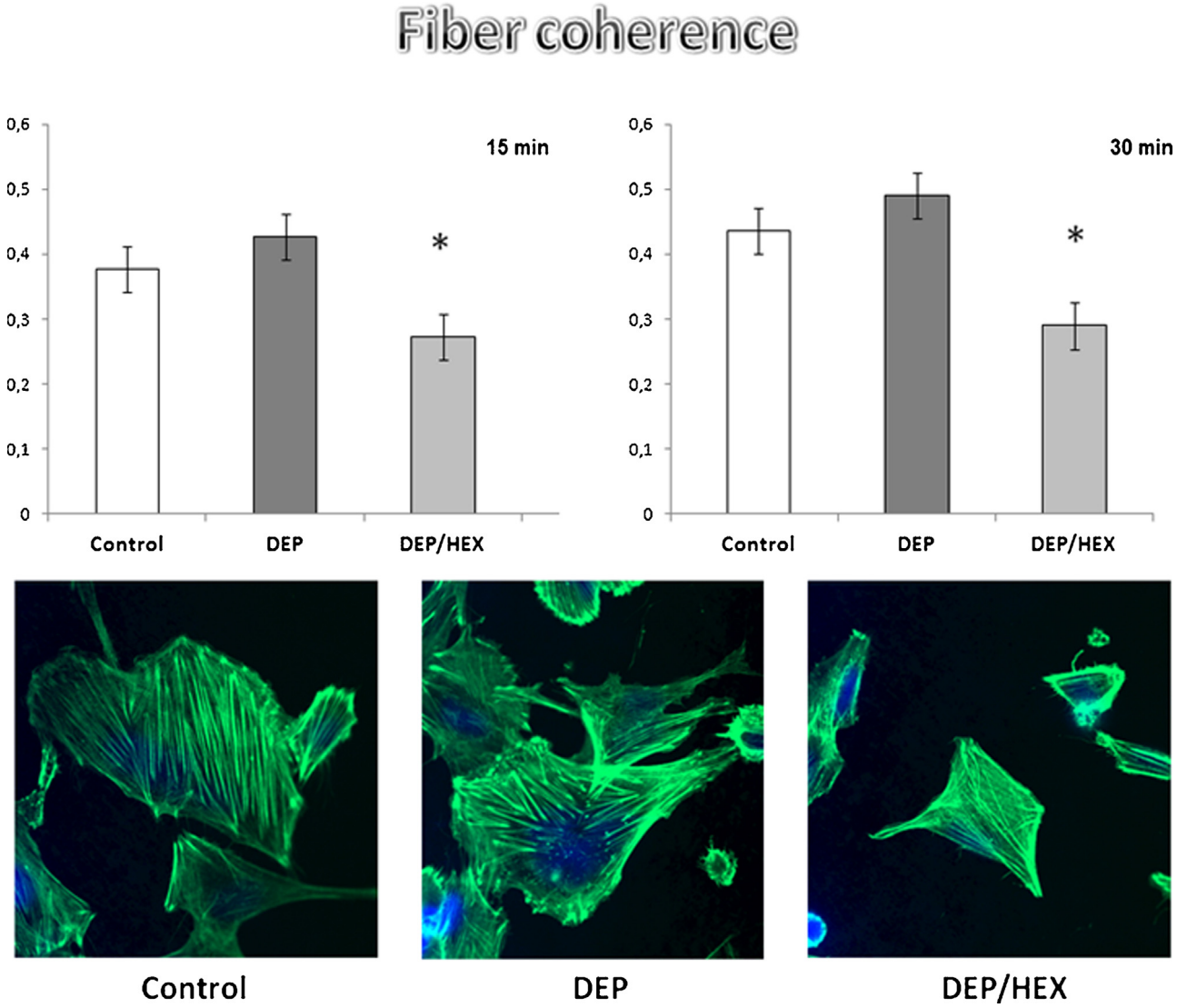

Fig. 4. Graphic representation of BEAS-2B shows fiber coherence after treatment with DEP crude and DEP/HEX at 15 and 30 min. Fiber coherence in crude DEP ($p = 0.001$) and in the control ($p = 0.001$) differed from DEP/HEX at 15 and 30 min.

cytoskeleton is involved in the transport of MAPKs over long distances within the cell (Wortzel and Seger, 2011).

According to Barros and Marshall (2005) and Tricker et al. (2011), pERK activation acts as pro-survival mechanism against the apoptotic effects of pJNK. We did not observe this situation in the DEP group because MTT decreased, but is possible that this result occurred in the case of cytoskeleton integrity. pJNK was found to be associated with MTT reduction, a relationship which suggests apoptosis (Tournier et al., 1997). According to Davis and Weston and Davis (2007), JNK is important in other forms of cell death, including necrosis and autophagy, because the mitochondria are a primary target of JNK-mediated pro-apoptotic signaling.

DEP/HEX removed a large fraction of the organic compounds of medium and low polarity. There was no expression of pERK, there was a peak in the expression of pJNK. In addition, LDH and viscoelasticity (G) increased, while fiber coherence decreased. According to Goberdhan and Wilson (1998), JNK activation has been implicated in cytoskeletal rearrangements, immune and cellular stress responses, growth arrest, and the regulation of apoptosis, all of which contributes to the surprising conclusion that a single signaling cascade may control both specific developmental events and general physiological responses to harmful stimuli. In our experiments, the reduction in fiber coherence and the increase in viscoelasticity both suggest that disorganization of the cytoskeleton is associated with rigid cells or rearrangements. In this context, the decrease in fiber coherence, (lack of alignment) suggests that pJNK does not translocate to the nucleus, where it could activate multiple transcription factors (such as apoptosis). Moreover, organic compound removal increases the bioavailability of some metals and causes the membrane damage observed in the increase of LDH.

In summary, it can be concluded that DEP/HEX induces subcellular alterations, such as changes in viscoelasticity, cell size, and cytoskeleton orientation through the differential activation of the MAPK family in bronchial epithelial cells. Considering the fact that the cells of the respiratory epithelium are the first line of defense between the body and environment in the protection against toxins, pathogens, and inhaled particulate matter, including DEP, our data contribute to a better understanding of the pathways leading to respiratory cell injury caused by DEP exposure.

The adverse findings detected after exposure to DEP fraction represent the toxic potential of diesel compounds, which could

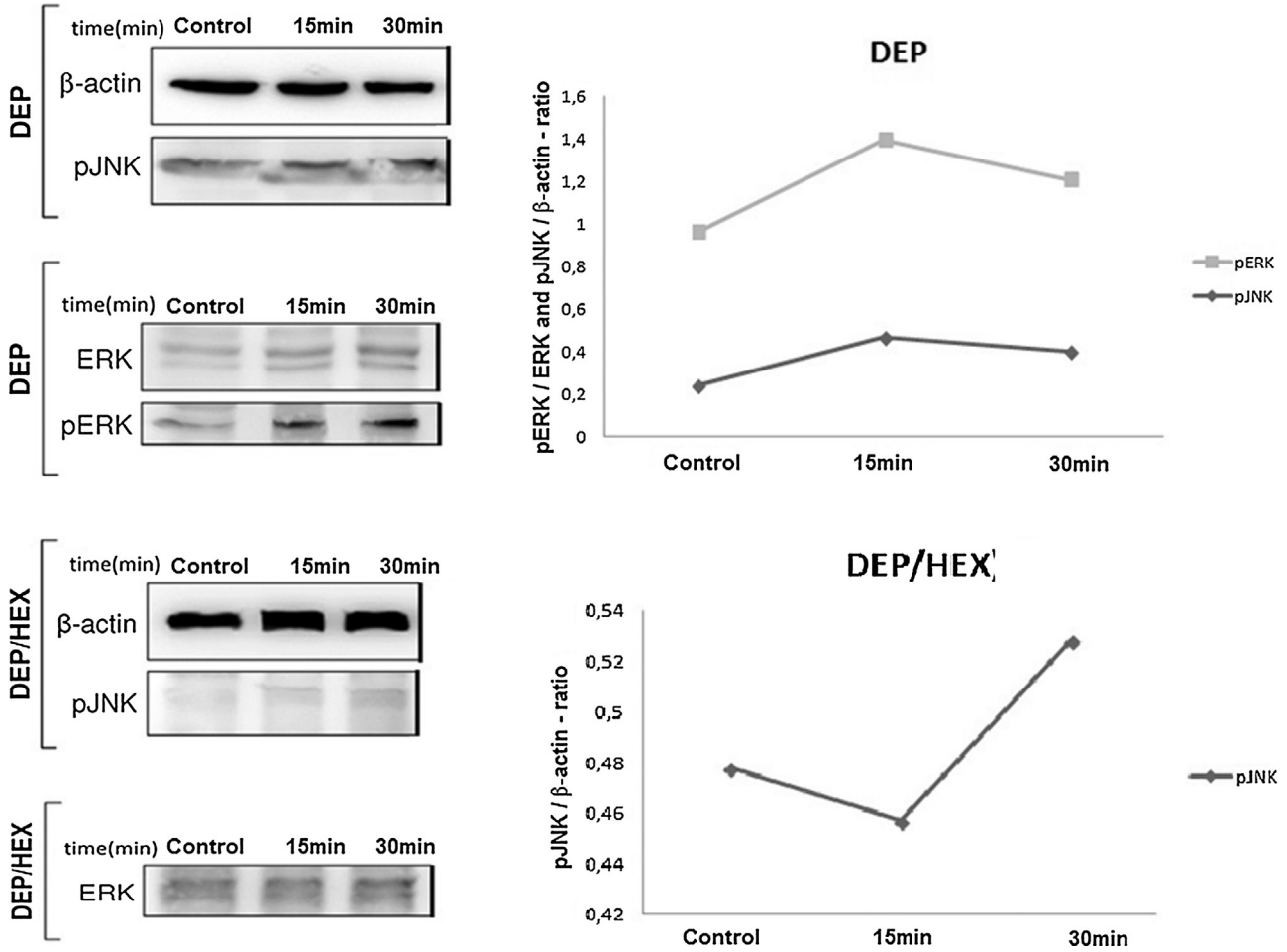

Fig. 5. Western blot showed the activation of MAPK (ERK and JNK) through phosphorylation in BEAS-2B cells. Phosphorylation of ERK (pERK) was observed after exposure to crude DEP increased over time. DEP/HEX did not cause ERK phosphorylation. JNK phosphorylation (pJNK) was observed between 15 and 30 min in crude DEP. When treated with DEP/HEX, the peak was not achieved until 30 min.

be a consequence of using poor quality fuel with low-technology engines.

Acknowledgments

This study was supported financially by Fundação de Amparo à Pesquisa do Estado de São Paulo – FAPESP (Process No. 2011/50334-7). We would like to thank Cristina Grandal for editing the figures, and Dr. Carla Lima, and Marcio José Ferreira (Instituto Butantã, São Paulo) for helping us with the cell culture. Finally, we would like to thank Dr. Monique Matsuda, Paloma G. Krempel, Dr. Mário Luiz Ribeiro Monteiro (LIM33), and Roger Chammas (LIM24) for their critical analysis, suggestions, and technical support in the laboratory.

References

Abou Chakra OR, Joyeux M, Nerriere E, Strub MP, Zmirou-Navier D. Genotoxicity of organic extracts of urban airborne particulate matter: an assessment within a personal exposure study. Chemosphere 2007;66(7):1375–81.

Altuğ H, Gaga EO, Döğeroğlu T, Ozden O, Ornektekin S, Brunekreef B, et al. Effects of air pollution on lung function and symptoms of asthma, rhinitis and eczema in primary school children. Environ Sci Pollut Res Int 2013;20:6455–67.

Araujo JA, Nel AE. Particulate matter and atherosclerosis: role of particle size, composition and oxidative stress. Part Fibre Toxicol 2009;6(1):24–42.

Ayres JG, Borm P, Cassee FR, Castranova V, Donaldson K, Ghio A, et al. Evaluating the toxicity of airborne particulate matter and nanoparticles by measuring oxidative stress potential – a workshop report and consensus statement. Inhal Toxicol 2008;20:75–99.

Barros JC, Marshall CJ. Activation of either ERK1/2 or ERK5 MAP kinase pathways can lead to disruption of the actin cytoskeleton. J Cell Sci 2005;118:1663–71.

Bayram H, Devalia JL, Sapsford RJ, Ohtoshi T, Miyabara Y, Sagai M, et al. The effect of diesel exhaust particles on cell function and release of inflammatory mediators from human bronchial epithelial cells in vitro. Am J Respir Cell Mol Biol 1998;18:441–8.

Berntsen P, Park CY, Rothen-Rutishauser B, Tsuda A, Sager TM, Molina RM, et al. Biomechanical effects of environmental and engineered particles on human airway smooth muscle cells. J R Soc Interface 2010;3:S331–40.

Bursac P, Lenormand G, Fabry B, Oliver M, Weitz DA, Viasnoff V, et al. Cytoskeletal remodelling and slow dynamics in the living cell. Nat Mater 2005;4:557–61.

Cakmak S, Dales R, Kauri LM, Mahmud M, Van Ryswyk K, Vanos J, et al. Metal composition of fine particulate air pollution and acute changes in cardiorespiratory physiology. Environ Pollut 2014;189:208–14.

Dinardo CL, Venturini G, Zhou EH, Watanabe IS, Campos LC, Dariolli R, et al. Variation of mechanical properties and quantitative proteomics of VSMC along the arterial tree. Am J Physiol Heart Circ Physiol 2013;15:H505–16.

Dreher K, Jurkat R, Kodanvanti U, Lehmann J, Winsett D, Costa D. Soluble transition metals mediate acute pulmonary injury and airway hyperresponsiveness induced by residual oil fly ash particles. Chest 1996;109:33S–4S.

Fabry B, Maksym GN, Butler JP, Glogauer M, Navajas D, Fredberg JJ. Scaling the microrheology of living cells. Phys Rev Lett 2001;87:102–48.

Fantl WJ, Johnson DE, WIlliams LT. Signalling by receptor tyrosine kinases. Annu Ver Biochem 1993;62:453–81.

Gan WQ, FitzGerald JM, Carlsten C, Sadatsafavi M, Brauer M. Associations of ambient air pollution with chronic obstructive pulmonary disease hospitalization and mortality. Am J Respir Crit Care Med 2013;187:721–7.

Ghio AJ, Silbajoris R, Carson JL, Samet JM. Biologic effects of oil fly ash. Environ Health Perspect 2002;110(suppl. 1):89–94.

Ghio AJ, Carraway MS, Madden MC. Composition of air pollution particles and oxidative stress in cells, tissues, and living systems. J Toxicol Environ Health B 2012;15(1):1–21.

Goberdhan DC, Wilson C. JNK, cytoskeletal regulator and stress response kinase? A Drosophila perspective. Bioessays 1998;20:1009–19.

Gurbani D, Bharti SK, Kumar A, Pandey AK, Ana GR, Verma A, et al. Polycyclic aromatic hydrocarbons and their quinones modulate the metabolic profile and induce DNA damage in human alveolar and bronchiolar cells. Int J Hyg Environ Health 2013;216(5):553–65.
Hill CS, Treisman R. Transcriptional regulation by extracellular signals: mechanisms and specificity. Cell 1995;80(2):199–211.
Hsu SO, Ito K, Lippmann M. Effects of thoracic and fine PM and their components on heart rate and pulmonary function in COPD patients. J Expo Sci Environ Epidemiol 2011;21(5):464–72.
Laks DM, Oliveira R, André P, Macchione M, Lemos M, Faffe DS, et al. Composition of diesel particles influences acute pulmonary toxicity: an experimental study in mice. Inhal Toxicol 2008;11:1037–42.
Li N, Wang M, Oberley TD, Sempf JM, Nel AE. Comparison of the pro-oxidative and proinflammatory effects of organic diesel exhaust particle chemicals in bronchial epithelial cells and macrophages. J Immunol 2002;169:4531–41.
Li N, Hao M, Phalen RF, Hinds WC, Nel AE. Particulate air pollutants and asthma: a paradigm for the role of oxidative stress in PM-induced adverse health effects. Clin Immunol 2003;109(3):250–65.
Li R, Ning Z, Cui J, Khalsa B, Ai L, Takabe W, et al. Ultrafine particles from diesel engines induce vascular oxidative stress via JNK activation. Free Radic Biol Med 2009;15:775–82.
Lim J, Limc C, Yu LE. Composition and size distribution of metals in diesel exhaust particulates. J Environ Monit 2009;11:1614–21.
Miraglia SG, Veras MM, Amato-Lourenço LF, Rodrigues-Silva F, Saldiva PH. Follow-up of the air pollution and the human male-to-female ratio analysis in Sao Paulo, Brazil: a times series study. BMJ Open 2013;26(3):7.
Ostro B, Roth L, Malig B, Marty M. The effects of fine particle components on respiratory hospital admissions in children. Environ Health Perspect 2009;117(3):475–80.
Papaharalambus CA, Griendling KK. Basic mechanisms of oxidative stress and reactive oxygen species in cardiovascular injury. Trends Cardiovasc Med 2007;17:48–54.
Park CY, Tambe D, Alencar AM, Trepat X, Zhou EH, Millet E, et al. Mapping the cytoskeletal prestress. Am J Physiol Cell Physiol 2010;298:C1245–52.
Pope CA, Dockery DW. Health effects of fine particulate air pollution: lines that connect. J Air Waste Manag Assoc 2006;56:709–42.
Rezakhaniha RA, Agianniotis JTC, Schrauwen A, Griffa D, Sage CVC, Bouten FN, et al. Experimental investigation of collagen waviness and orientation in the arterial adventitia using confocal laser scanning microscopy. Biomech Model Mechanobiol 2012;11:461–73.
Riss TL, Moravec RA. Use of multiple assay endpoints to investigate the effects of incubation time, dose of toxin, and plating density in cell-based cytotoxicity assays. Assay Drug Dev Technol 2004;2:51–62.
Romão R, Pereira LAA, Saldiva PHN, Pinheiro PM, Braga ALF, Martins LC. The relationship between low birth weight and exposure to inhalable particulate matter. Cad Saúde Pública 2013;29:1101–8.
Saldiva PH, Clarke RW, Coull BA, Stearn RC, Lawrence J, Murthy GG, et al. Lung inflammation induced by concentrated ambient air particles is related to particle composition. Am J Respir Crit Care Med 2002;165:1610–7.
Schikowski T, Mills IC, Anderson HR, Cohen A, Hansell A, Kauffmann F, et al. Ambient air pollution – a cause for COPD? Eur Respir J 2014;43:250–63.
Seriani R, Junqueira MS, de Toledo AC, Martins MA, Seckler M, Alencar AM, et al. Diesel exhaust particulates affect cell signaling, mucin profiles, and apoptosis in trachea explants of Balb/C mice. Environ Toxicol 2014;29.
Seriani R, Junqueira MS, Toledo AC, Corrêa AT, Silva LF, Martins MA, et al. Organic and inorganic fractions of diesel exhaust particles produce changes in mucin profile of mouse trachea explants. J Toxicol Environ Health A 2015;78(4):215–25.
Sérgio-Chiarelli P, Amador Pereira LA, Saldiva PH, Ferreira-Filho C, Bueno-Garcia ML, Ferreira-Braga AL, et al. The association between air pollution and blood pressure in traffic controllers in Santo André, São Paulo, Brazil. Environ Res 2011;111:650–5.
Tamura E, Fernandes K, Marçola PA, Cruz-Machado M, Markus SSRP. Long-lasting priming of endothelial cells by plasma melatonin levels. PLoS ONE 2010;5:e13958.
Tournier C, Thomas G, Pierre J, Jacquemin C, Pierre M, Saunier B. Mediation by arachidonic acid metabolites of the H_2O_2-induced stimulation of mitogen-activated protein kinases (extracellular-signal-regulated kinase and c-Jun NH_2-terminal kinase). Eur J Biochem 1997;244(2):587–95.
Totlandsdal AI, Cassee FR, Schwarze P, Refsnes M, Låg M. Diesel exhaust particles induce CYP1A1 and pro-inflammatory responses via differential pathways in human bronchial epithelial cells. Part Fibre Toxicol 2010;16(7):41.
Totlandsdal AI, Låg M, Lilleaas E, Cassee F, Schwarze P. Differential proinflammatory responses induced by diesel exhaust particles with contrasting PAH and metal content. Environ Toxicol 2013;31.
Tricker E, Arvand A, Kwan R, Chen GY, Gallagher E, Cheng G. Apoptosis induced by cytoskeletal disruption requires distinct domains of MEKK1. PLoS ONE 2011;25:e17310.
Zhou EH, Xu F, Quek ST, Lim CT. A power-law rheology-based finite element model for single cell deformation. Biomech Model Mechanobiol 2012;11:1075–84.
Weston CR, Davis RJ. The JNK signal transduction pathway. Curr Opin Cell Biol 2007;19:142–9.
Wichmann HE. Diesel exhaust particles. Inhal Toxicol 2007;19:241–4.
Wortzel I, Seger R. The ERK cascade: distinct functions within various subcellular organelles. Genes Cancer 2011;3:195–209.
Wu Y, Yu T, Gilbertson TA, Zhou A, Xu H, Nguyen KT. Biophysical assessment of single cell cytotoxicity: diesel exhaust particle-treated human aortic endothelial cells. PLoS ONE 2012;7:e36885.
Yorifuji T, Kashima S. Air pollution: another cause of lung cancer. Lancet Oncol 2013;14:788–99.
Yoshizaki K, Brito JM, Toledo AC, Nakagawa NK, Piccin VS, Junqueira MS, et al. Subchronic effects of nasally instilled diesel exhaust particulates on the nasal and airway epithelia in mice. Inhal Toxicol 2010;22:610–7.
Zhou J, Ito K, Lall R, Lippmann M, Thurston G. Time-series analysis of mortality effects of fine particulate matter components in Detroit and Seattle. Environ Health Perspect 2010;119(4):461–6.